

**Two-Pole Nature of the  $\Lambda(1405)$  Resonance from Lattice QCD**

John Bulava<sup>1</sup>, Bárbara Cid-Mora<sup>2</sup>, Andrew D. Hanlon<sup>3</sup>, Ben Hörz<sup>4</sup>, Daniel Mohler<sup>5,2</sup>, Colin Morningstar<sup>6</sup>,  
Joseph Moscoso<sup>7</sup>, Amy Nicholson<sup>7</sup>, Fernando Romero-López<sup>8</sup>,  
Sarah Skinner<sup>6</sup>, and André Walker-Loud<sup>9</sup>

(Baryon Scattering (BaSc) Collaboration)

<sup>1</sup>Deutsches Elektronen-Synchrotron (DESY), Platanenallee 6, 15738 Zeuthen, Germany

<sup>2</sup>GSI Helmholtz Centre for Heavy Ion Research, Darmstadt 64291, Germany

<sup>3</sup>Physics Department, Brookhaven National Laboratory, Upton, New York 11973, USA

<sup>4</sup>Intel Deutschland GmbH, Dornacher Strasse 1, 85622 Feldkirchen, Germany


<sup>5</sup>Institut für Kernphysik, Technische Universität Darmstadt, Schlossgartenstrasse 2, 64289 Darmstadt, Germany

<sup>6</sup>Department of Physics, Carnegie Mellon University, Pittsburgh, Pennsylvania 15213, USA

<sup>7</sup>Department of Physics and Astronomy, University of North Carolina, Chapel Hill, North Carolina 27516-3255, USA

<sup>8</sup>Center for Theoretical Physics, Massachusetts Institute of Technology, Cambridge, Massachusetts 02139, USA

<sup>9</sup>Nuclear Science Division, Lawrence Berkeley National Laboratory, Berkeley, California 94720, USA

 (Received 28 July 2023; revised 15 November 2023; accepted 7 December 2023; published 30 January 2024)

This Letter presents the first lattice QCD computation of the coupled channel  $\pi\Sigma\text{-}\bar{K}N$  scattering amplitudes at energies near 1405 MeV. These amplitudes contain the resonance  $\Lambda(1405)$  with strangeness  $S = -1$  and isospin, spin, and parity quantum numbers  $I(J^P) = 0(1/2^-)$ . However, whether there is a single resonance or two nearby resonance poles in this region is controversial theoretically and experimentally. Using single-baryon and meson-baryon operators to extract the finite-volume stationary-state energies to obtain the scattering amplitudes at slightly unphysical quark masses corresponding to  $m_\pi \approx 200$  MeV and  $m_K \approx 487$  MeV, this study finds the amplitudes exhibit a virtual bound state below the  $\pi\Sigma$  threshold in addition to the established resonance pole just below the  $\bar{K}N$  threshold. Several parametrizations of the two-channel  $K$  matrix are employed to fit the lattice QCD results, all of which support the two-pole picture suggested by SU(3) chiral symmetry and unitarity.

DOI: [10.1103/PhysRevLett.132.051901](https://doi.org/10.1103/PhysRevLett.132.051901)

*Introduction.*—The strong nuclear force is described by quantum chromodynamics (QCD) which governs the dynamics and interactions of quarks and gluons. Because of an important property of QCD known as asymptotic freedom, the use of perturbation theory is useful for QCD scattering calculations at very high energies. The binding of quarks and gluons to form hadrons, such as protons and neutrons, is a low-energy phenomenon of QCD, requiring a nonperturbative calculational technique. Such techniques are difficult to apply, so understanding the hadron spectrum of QCD remains an important outstanding issue for the standard model of particle physics. In particular, resonances such as the  $\Lambda(1405)$  resonance defy the naive quark-model picture

of baryons and mesons. In this Letter, a Markov-chain Monte Carlo method using QCD formulated on a space-time lattice is applied to shed light on the puzzling hadron resonance structure in the region of the  $\Lambda(1405)$ .

The history of the  $\Lambda(1405)$  resonance began in Refs. [1,2] which suggested that the low-energy  $K^-p$  amplitude measured in bubble chamber experiments implies a resonance in the  $\pi^-\Sigma^+$  spectrum just below the  $K^-p$  threshold. The intervening decades have witnessed considerable experimental progress in this system [3,4], but a consensus about whether there is a single resonance or two nearby resonance poles in this energy region has not yet been reached. This is evidenced by the most recent Particle Data Group review [5] which lists an additional  $\Lambda(1380)$  resonance pole with lower confidence. An improved determination of the  $K^-p$  scattering length [6] was enabled by measurements of the energy shift and width of kaonic hydrogen by the SIDDHARTHA Collaboration at DAΦNE [7]. The angular analysis of the process  $\gamma + p \rightarrow K^+ + \Sigma + \pi$  by the CLAS Collaboration at JLab determined the line shapes [8] and the spin parity quantum

---

Published by the American Physical Society under the terms of the [Creative Commons Attribution 4.0 International license](https://creativecommons.org/licenses/by/4.0/). Further distribution of this work must maintain attribution to the author(s) and the published article's title, journal citation, and DOI. Funded by SCOAP<sup>3</sup>.

numbers [9]  $J^P = 1/2^-$ . The CLAS data have been analyzed in Refs. [10,11], which suggest the existence of two isoscalar poles. Recent data from the BGOOD Collaboration [12] and a preliminary study by the GlueX Collaboration [13] also support the two-pole scenario. Similarly, interhadron potentials determined by the ALICE Collaboration using the “femtoscopy” approach favor the two-pole picture [14]. However, recent data from J-PARC is successfully described by a single pole [15] and a combined analysis in Ref. [16] concludes that a single resonance sufficiently describes the experimental data, without ruling out the two-pole description.

On the theoretical side, the relatively low mass and quantum numbers of the  $\Lambda(1405)$  resonance are difficult to accommodate in constituent quark models [17]. However, some insight is gained from SU(3) chiral effective theory [18–20]. The leading-order interaction between the octet of Goldstone bosons and (ground-state) octet baryons [21,22] predicts an attractive interaction in both the flavor-SU(3) singlet and octet combinations. After employing a unitarization procedure, this attraction leads to two poles in the scattering matrix analytically continued to complex center-of-mass energies [23]. Despite the agreement of nearly all chiral approaches (which are reviewed in Refs. [24–26]) on the two-pole scenario, the position of the lower pole remains somewhat poorly constrained [5]. Recent theoretical works about the  $\Lambda(1405)$  resonance can be found in Refs. [27–34].

Lattice QCD is a first-principles method that can be used to unambiguously determine the nature of the  $\Lambda(1405)$  resonance and provide two unique insights. First, the elastic  $\pi\Sigma$  scattering amplitude can be computed directly below the  $\bar{K}N$  threshold. This process is difficult to access experimentally and lattice results may help identify and constrain a second lower pole. Second, the motion of the poles in the complex plane upon varying the  $u$ ,  $d$ , and  $s$  quark masses away from their physical values provides additional input to future chiral effective theory analyses [35,36].

The computation of real-time two-to-two scattering amplitudes below three-hadron thresholds from imaginary-time lattice QCD calculations is well developed and relies on the finite-volume spectrum of interacting two-hadron states [37–44]. Previous lattice QCD computations of the  $\Lambda(1405)$  resonance have not computed scattering amplitudes and instead aimed only to isolate the lowest finite-volume energy eigenstate using single-baryon three-quark interpolating fields [45–53]. Using only such operators is known to be insufficient to extract scattering information, such as scattering amplitudes and pole locations. The  $\bar{K}N$  scattering length for  $I = 0$  has been computed long ago using the quenched approximation [54], but mixing with the kinematically open  $\pi\Sigma$  channel was neglected. The  $\pi\Sigma$  and  $\bar{K}N$  scattering lengths in other (nonsinglet) flavor and isospin combinations not directly

relevant for the  $\Lambda(1405)$  resonance have been computed in Refs. [55–57].

This work computes the isospin  $I = 0$  and strangeness  $S = -1$  coupled-channel  $\pi\Sigma$ - $\bar{K}N$  scattering amplitudes below the  $\pi\pi\Lambda$  threshold from lattice QCD for the first time. A single ensemble of gauge configurations with dynamical  $u$ ,  $d$ , and  $s$  quarks is employed with pion and kaon masses of  $m_\pi \approx 200$  MeV and  $m_K \approx 487$  MeV, respectively, which deviate slightly from their physical values  $m_\pi^{\text{phys}} \approx 140$  MeV and  $m_K^{\text{phys}} \approx 495$  MeV. The  $u$  and  $d$  quark masses are set to be equal and electroweak interactions are neglected, so isospin is a good quantum number. The main result of this work is a set of parametrizations of the amplitudes which are constrained by fits to the finite-volume energy spectrum. These parametrizations can accommodate zero, one, or two poles, but when fit to the lattice results and analytically continued to the complex-energy plane, they all confirm the presence of two poles, the positions of which vary little and are consistent with predictions from chiral effective theory. Our use of  $m_\pi > m_\pi^{\text{phys}}$  moves the lower pole just below the  $\pi\Sigma$  threshold leading to its unambiguous identification as a virtual bound state. The higher pole near the  $\bar{K}N$  threshold is also clearly present.

This Letter provides a summary of the computation while technical details are left to a companion paper [58]. The main result is Fig. 1, which shows fits to the finite-volume spectrum using all parametrizations of the coupled-channel amplitude and the associated pole positions. Statistical errors are shown for the parametrization with the lowest Akaike information criterion (AIC) value.

*Determination of finite-volume energies.*—The ensemble of gauge configurations and algorithm for evaluating correlation functions are briefly reviewed here and discussed more deeply in the companion paper. The  $N_f = 2 + 1$  QCD gauge configurations comprise the “D200” ensemble generated by the Coordinated Lattice Simulations (CLS) consortium [59] which is detailed in Table I. The lattice spacing is determined in Ref. [60] and updated in Ref. [61]. All correlation matrices are computed using the stochastic-LapH [62] implementation of Ref. [63]. The flexibility afforded by the source-sink factorization and subsequent computation of correlators via optimized tensor contractions [64] is particularly advantageous for large Hermitian correlation matrices containing single-baryon,  $\pi\Sigma$ , and  $\bar{K}N$  interpolating operators.

The determination of finite-volume stationary-state energies is also discussed in detail in the companion paper and summarized here. The interaction shift  $\Delta E_{\text{lab}}$  of a lab-frame energy from a nearby noninteracting energy is extracted from a single-state fit to the ratio of a diagonalized correlation function over the product of correlators for the individual constituents of the nearby noninteracting energy. The diagonalization of the correlation matrices is done by solving a generalized eigenvalue problem (GEVP)

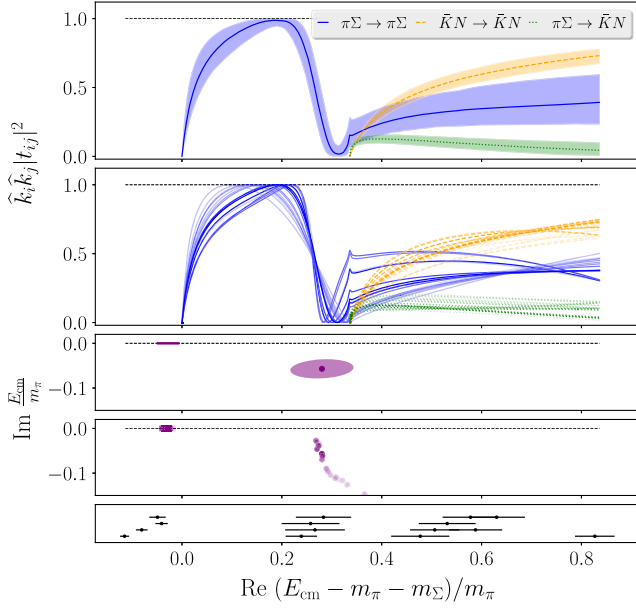


FIG. 1. The  $I = 0$  and  $S = -1$  coupled-channel  $\pi\Sigma\text{-}\bar{K}N$  amplitude computed on a single lattice QCD gauge-field ensemble with  $m_\pi \approx 200$  MeV as a function of the energy difference to the  $\pi\Sigma$  threshold in the center-of-mass frame. The upper panel shows the transition matrix elements, defined in Eq. (4), using the  $K$ -matrix parametrization with the lowest AIC constrained by the finite-volume spectrum in the bottom panel. The second panel shows the model variation for the same quantities using several parametrizations. The third and fourth panels show the position of poles in the complex center-of-mass energy ( $E_{\text{cm}}$ ) plane on the sheets closest to the physical one: using the parametrization with the lowest AIC (third panel), and for several parametrizations (fourth panel). In the second and fourth panel, the transparency of each line and corresponding pair of pole positions are proportional to  $\exp[-(\text{AIC} - \text{AIC}_{\text{min}})/2]$ , where  $\text{AIC}_{\text{min}}$  is the lowest AIC corresponding to the fit in Eq. (3), which is also shown in the top panel. The subscripts  $i, j$  index the two open scattering channels. In the lowest panel, the lattice QCD energy levels that serve as input to the amplitude analyses are displayed. For clarity, these energy levels are displaced vertically by the total spatial momentum  $d^2$  defined below Eq. (1).

as described in Ref. [63]. We have verified the insensitivity of our extracted energies to reasonable variations of the GEVP parameters, the use of different nearby noninteracting levels, and different fit forms. An example energy determination is shown in Fig. 2 for the ground state of the  $G_{1u}(0)$  irreducible representation (irrep), which predominantly contains the

TABLE I. Parameters of the D200 ensemble [59]. The lattice dimensions in space and time ( $L$  and  $T$ ), as well as the mass of the pion ( $m_\pi$ ) and kaon ( $m_K$ ) are given in units of the lattice spacing  $a$ . In pion mass units, the size of the box is  $m_\pi L = 4.181(16)$ .

$a$ (fm)	$(L/a)^3 \times T/a$	$am_\pi$	$am_K$
0.0633(4)(6)	$64^3 \times 128$	0.065 33(25)	0.156 02(16)

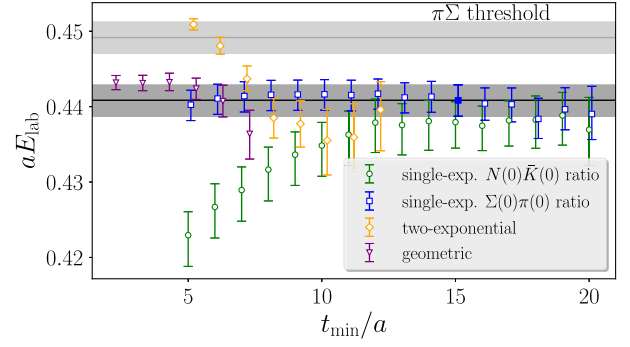


FIG. 2. Example determination of a finite-volume stationary-state energy, illustrating the sensitivity of the fitted energy to the lower end of the fit range ( $t_{\text{min}}$ ) for the lowest level of the  $G_{1u}(0)$  irrep. Each set of points corresponds to a different fit form. The two-exponential and geometric [63] fits are performed to the diagonalized correlation function only. The single-exponential ratio fits are performed to the same correlator divided by either the product  $\bar{K}(0)N(0)$  or  $\pi(0)\Sigma(0)$  of correlators, and the lab frame energy  $aE_{\text{lab}}$  is reconstructed from the interaction shifts. The dark horizontal band and filled symbol denote the chosen fit.

parity-odd,  $s$ -wave scattering system. All levels used to constrain the amplitude are shown in Fig. 3.

*Scattering amplitude determination.*—In lattice QCD, scattering amplitudes below three-hadron thresholds are inferred from finite-volume spectra [37–44] using the relationship [65]

$$\det[\tilde{K}^{-1}(E_{\text{cm}}) - B^P(E_{\text{cm}})] = 0. \quad (1)$$

The matrix  $\tilde{K}$  is related to the usual scattering  $K$  matrix (normalized such that the single-channel equivalent of  $\tilde{K}^{-1}$  is the  $s$ -wave  $k \cot \delta_0$ ), and the “box matrix”  $B^P$  for a particular total momentum  $\mathbf{P} = (2\pi/L)\mathbf{d}$  (with  $\mathbf{d} \in \mathbb{Z}^3$ )

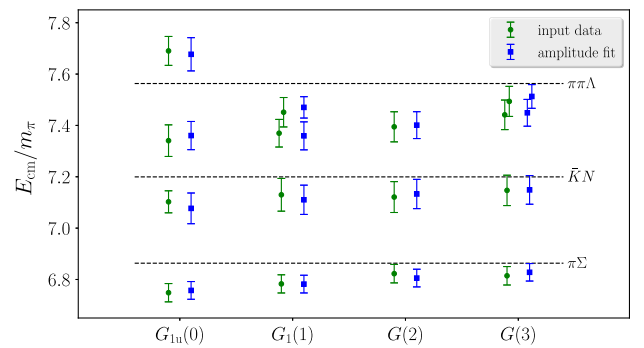


FIG. 3. Finite-volume spectrum in the center-of-mass frame used as input data to constrain parametrizations of the coupled-channel  $\pi\Sigma\text{-}\bar{K}N$  scattering amplitude. Each column corresponds to a particular irrep  $\Lambda(d^2)$  of the little group of total momentum  $\mathbf{P}^2 = (2\pi/L)^2 d^2$ . Only irreps where the  $\ell = 0$  partial wave contributes are included. Dashed lines indicate various thresholds, as labeled. Model energies from the resultant scattering-amplitude fit are given by blue squares.

encodes the reduction in symmetry due to the finite toroidal spatial volume.  $E_{\text{cm}}$  denotes center-of-mass energy. Equation (1) ignores terms which are suppressed exponentially with the spatial extent  $L$ . For scattering between baryons and pseudoscalar mesons, the  $K$  matrix does not mix different  $J^P$ , but does couple the  $\pi\Sigma$  and  $\bar{K}N$  channels. By contrast, the box matrix is diagonal in the two scattering channels, but mixes partial waves.  $B^P$  is, however, block diagonal in the basis given by irreps of the finite-volume little group of momentum  $P$ . Demanding a vanishing determinant in one of these infinite-dimensional blocks provides a relationship between the  $K$ -matrix and the finite-volume spectrum in a particular irrep. In practice, partial waves with orbital angular momentum  $\ell > \ell_{\text{max}}$  are neglected; here  $\ell_{\text{max}} = 0$  is chosen in both the  $\pi\Sigma$  and  $\bar{K}N$  channels. The systematic error due to this is estimated by considering  $\ell_{\text{max}} = 1$ , and found to be insignificant for the near-threshold energy region relevant here. Specifically, the effect of including additional waves with  $\ell = 1$  leads to shifts that are significantly smaller than the statistical uncertainties in fit results for the  $\ell = 0$   $K$  matrix. Levels from all irreps in Table 1 of Ref. [63] to which the  $J^P = 1/2^-$  partial wave contributes are employed, as well as one level each from the  $G_{1g}(0)$ ,  $F_1(3)$ , and  $F_2(3)$  irreps for the  $\ell_{\text{max}} = 1$  check. All elements of  $B^P$  required for this work are given in Ref. [65].

For  $\ell_{\text{max}} = 0$ , the finite-volume spectrum shown in Fig. 3 constrains the coupled-channel scattering amplitude via Eq. (1) at center-of-mass energies near the  $\pi\Sigma$  and  $\bar{K}N$  thresholds. The effective range expansion (ERE) is used to parametrize the  $K$  matrix

$$\frac{E_{\text{cm}}}{m_\pi} \tilde{K}_{ij} = A_{ij} + B_{ij} \Delta_{\pi\Sigma}, \quad (2)$$

where  $A_{ij}$  and  $B_{ij}$  are symmetric and real coefficients with  $i$  and  $j$  denoting either of the two scattering channels (channel 0 is  $\pi\Sigma$  and channel 1 is  $\bar{K}N$ ). Moreover,  $\Delta_{\pi\Sigma} = [E_{\text{cm}}^2 - (m_\pi + m_\Sigma)^2] / (m_\pi + m_\Sigma)^2$  labels the distance to the  $\pi\Sigma$  threshold. The parameters, which are the elements of the  $A$  and  $B$  matrices, are determined from fits to the lattice QCD results using the spectrum method [66]. Similar fits are performed with variations of the above parametrization: an ERE for  $\tilde{K}^{-1}$ , removing the factor of  $E_{\text{cm}}$  in Eq. (2), parametrizations inspired by the Weinberg-Tomozawa potential [19], or using the Blatt-Biedenharn [67] form. The effect of fixing some (or all) of the elements of  $B$  to zero is also explored.

The correlated- $\chi^2$  of the above fits is defined by comparing the center-of-mass interaction shifts  $\Delta E_{\text{cm}}$  obtained from the model with those determined from the ratio fits with a particular choice of the noninteracting levels. The fit with the lowest AIC value is a four-parameter fit to Eq. (2). The result is

$$\begin{aligned} A_{00} &= 4.1(1.8), & A_{11} &= -10.5(1.1), \\ A_{01} &= 10.3(1.5), & B_{01} &= -29(18), \end{aligned} \quad (3)$$

with fixed  $B_{00} = B_{11} = 0$  and  $\chi^2 = 10.52$  for 11 degrees of freedom. This fit is shown in Fig. 1. All statistical uncertainties and correlations are taken into account using the bootstrap method with 800 samples.

*Analytic structure of the amplitude.*—The various parametrizations discussed above constrain the energy dependence of the amplitudes near the finite-volume energies, even if they do not accommodate left-hand (cross-channel) cuts. Knowledge over this limited range enables the analytic continuation of the scattering amplitude (denoted  $\mathcal{T}$ ) to complex  $E_{\text{cm}}$  and the identification of poles close to the real axis on sheets adjacent to the physical one.

The  $K$  matrix, the  $J^P = 1/2^-$  scattering amplitude  $\mathcal{T}$ , and the normalized amplitude  $t$  shown in Fig. 1 are related by

$$t^{-1} = \frac{8\pi E_{\text{cm}}}{m_\pi} \mathcal{T}^{-1} = \tilde{K}^{-1} - i\hat{k}, \quad (4)$$

where  $m_\pi \hat{k} = \text{diag}(k_{\pi\Sigma}, k_{\bar{K}N})$ ,

$$k_{\pi\Sigma}^2 = \frac{1}{4E_{\text{cm}}^2} \lambda(E_{\text{cm}}^2, m_\pi^2, m_\Sigma^2).$$

Here,  $\lambda(x, y, z)$  is the Källén function [68] and  $k_{\bar{K}N}$  is defined similarly. Analytic continuation of the coupled channel  $\pi\Sigma$ - $\bar{K}N$  amplitude involves four different Riemann sheets, each labeled by the sign of the imaginary parts of  $(k_{\pi\Sigma}, k_{\bar{K}N})$ , with  $(+, +)$  denoting the physical sheet. Complex poles in the scattering amplitude correspond to vanishing eigenvalues in the right-hand side of Eq. (4), and are determined numerically. In the vicinity of a pole, the divergent part of the amplitude is

$$t = \frac{m_\pi}{E_{\text{cm}} - E_{\text{pole}}} \begin{pmatrix} c_{\pi\Sigma}^2 & c_{\pi\Sigma} c_{\bar{K}N} \\ c_{\pi\Sigma} c_{\bar{K}N} & c_{\bar{K}N}^2 \end{pmatrix} + \dots, \quad (5)$$

where the (complex) residues  $c_{\pi\Sigma}$  and  $c_{\bar{K}N}$  denote the coupling of the resonance pole to each channel.

Two poles are found on the  $(-, +)$  sheet, which is the one closest to physical scattering in the region between the two thresholds. Their locations are

$$\begin{aligned} E_1 &= 1392(9)(2)(16) \text{ MeV}, \\ E_2 &= [1455(13)(2)(17) - i11.5(4.4)(4)(0.1)] \text{ MeV}, \end{aligned} \quad (6)$$

and their couplings

$$\left| \frac{c_{\pi\Sigma}^{(1)}}{c_{\bar{K}N}^{(1)}} \right| = 1.9(4)(6), \quad \left| \frac{c_{\pi\Sigma}^{(2)}}{c_{\bar{K}N}^{(2)}} \right| = 0.53(9)(10). \quad (7)$$

The first uncertainty is statistical, the second accounts for parametrization dependence and for the pole positions, the

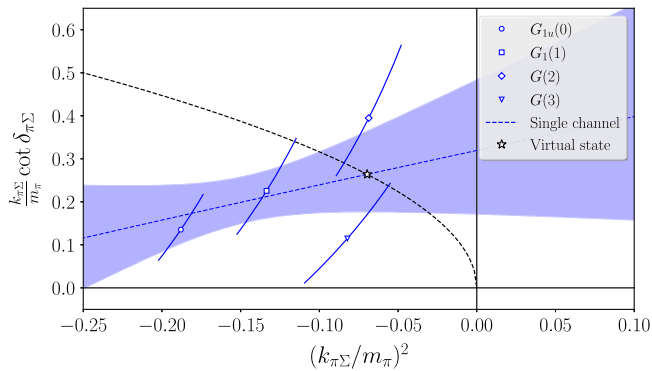


FIG. 4. The elastic  $\pi\Sigma$  amplitude near threshold. The points are obtained from Eq. (1) using a single channel and  $\ell_{\max} = 0$ . The shaded band denotes a fit of the four levels shown to a two-parameter effective range expansion. A pole on the real axis in the second Riemann sheet (a virtual bound state) occurs when  $k_{\pi\Sigma} \cot \delta_{\pi\Sigma} - ik_{\pi\Sigma} = 0$  below threshold. This is where the black dashed line intersects the fit.

third comes from the uncertainty in the lattice spacing in Table I. Two poles are present for all parametrizations of the  $K$  matrix. The pole at  $E_1$  is likely a virtual bound state, except in 0.5% of bootstrap samples where it is located on the physical sheet and thus a bound state, while the one at  $E_2$  is a resonance. The first pole has a stronger coupling to the  $\pi\Sigma$  channel, while for the second, the hierarchy is reversed, a pattern also predicted by chiral unitary models. Further confirmation of the existence of the lower pole as a virtual bound state comes from a single-channel analysis of the energy levels near the  $\pi\Sigma$  threshold, as shown in Fig. 4.

**Conclusion.**—This study of  $\pi\Sigma$ - $\bar{K}N$  scattering in the  $\Lambda(1405)$  resonance region is the first coupled-channel meson-baryon scattering amplitude determined from lattice QCD. Hermitian correlation matrices using both single-baryon and meson-baryon interpolating operators for a variety of different total momenta and irreducible representations were used. The analytic continuation of the amplitudes into the complex center-of-mass energy plane is stabilized by finite-volume energies just below the  $\pi\Sigma$  and  $\bar{K}N$  thresholds and clearly exhibits two poles. At a slightly heavier-than-physical pion mass of  $m_\pi \approx 200$  MeV, the lower pole is a virtual bound state below the  $\pi\Sigma$  threshold and the higher a resonance just below the  $\bar{K}N$  threshold. Because of our use of  $m_\pi > m_\pi^{\text{phys}}$ , the real parts of the pole positions in Eq. (6) are somewhat larger than those determined at the physical point from experiment using chiral approaches [5], which lie within the ranges  $\text{Re}E_1 = 1325\text{--}1380$  MeV and  $\text{Re}E_2 = 1421\text{--}1434$  MeV. Importantly, this qualitative consistency supports the two-pole picture predicted by chiral symmetry and unitarity.

Future work with this system includes moving to physical quark masses which requires the consideration of three particle effects, but this should not present a major problem in the region relevant for the  $\Lambda(1405)$ . Estimating

residual finite-volume and lattice spacing effects is also planned. Studying this system along the quark-mass trajectory toward the SU(3)-symmetric point will also test the motion of the pole positions predicted by chiral effective theories. Finally, this work opens the door to investigations of other baryon resonances, such as the  $N(1535)$ ,  $\Lambda(1670)$ ,  $\Sigma(1620)$ , and  $\Xi(1620)$ .

NumPy [69], Matplotlib [70], and the CHROMA software suite [71] were used for analysis, plotting, and correlator evaluation.

We acknowledge helpful discussions with R. J. Hudspith, A. Jackura, M. Mai, and M. Lutz. We are also grateful to S. Kuberski for providing reweighting factors for the D200 ensemble, as computed according to Ref. [72]. We thank our colleagues within the CLS consortium for sharing ensembles. Computations were carried out on Frontera [73] at the Texas Advanced Computing Center (TACC), and at the National Energy Research Scientific Computing Center (NERSC), a U.S. Department of Energy (DOE) Office of Science User Facility located at Lawrence Berkeley National Laboratory, operated under Contract No. DE-AC02-05CH11231 using NERSC Awards No. NP-ERCAP0005287, No. NP-ERCAP0010836, and No. NP-ERCAP0015497. This work was supported in part by the U.S. National Science Foundation under Awards No. PHY-1913158 and No. PHY-2209167 (C. M., S. S.), the Faculty Early Career Development Program (CAREER) under Award No. PHY-2047185 (A. N.) and by the Graduate Research Fellowship Program under Grant No. DGE-2040435 (J. M.), the U.S. Department of Energy, Office of Science, Office of Nuclear Physics, under Grant Contracts No. DE-SC0011090 and No. DE-SC0021006 (F. R.-L.), No. DE-SC0012704 (A. D. H.), No. DE-AC02-05CH11231 (A. W.-L.) and within the framework of Scientific Discovery through Advanced Computing (SciDAC) award “Fundamental Nuclear Physics at the Exascale and Beyond” (A. D. H.), the Mauricio and Carlota Botton Fellowship (F. R.-L.), and the Heisenberg Programme of the Deutsche Forschungsgemeinschaft (DFG, German Research Foundation) Project No. 454605793 (D. M.).

- [1] R. H. Dalitz and S. F. Tuan, Possible resonant state in pion-hyperon scattering, *Phys. Rev. Lett.* **2**, 425 (1959).
- [2] R. H. Dalitz and S. F. Tuan, The phenomenological representation of  $\bar{K}$ -nucleon scattering and reaction amplitudes, *Ann. Phys. (N.Y.)* **10**, 307 (1960).
- [3] T. Hyodo and D. Jido, The nature of the  $\Lambda(1405)$  resonance in chiral dynamics, *Prog. Part. Nucl. Phys.* **67**, 55 (2012).
- [4] T. Hyodo and M. Niiyama, QCD and the strange baryon spectrum, *Prog. Part. Nucl. Phys.* **120**, 103868 (2021).
- [5] R. L. Workman *et al.* (Particle Data Group), Review of particle physics, *Prog. Theor. Exp. Phys.* **2022**, 083C01 (2022).

- [6] U. G. Meissner, U. Raha, and A. Rusetsky, Spectrum and decays of kaonic hydrogen, *Eur. Phys. J. C* **35**, 349 (2004).
- [7] M. Bazzi *et al.* (SIDDHARTA Collaboration), A new measurement of kaonic hydrogen x-rays, *Phys. Lett. B* **704**, 113 (2011).
- [8] K. Moriya *et al.* (CLAS Collaboration), Measurement of the  $\Sigma\pi$  photoproduction line shapes near the  $\Lambda(1405)$ , *Phys. Rev. C* **87**, 035206 (2013).
- [9] K. Moriya *et al.* (CLAS Collaboration), Spin and parity measurement of the  $\Lambda(1405)$  baryon, *Phys. Rev. Lett.* **112**, 082004 (2014).
- [10] M. Mai and U.-G. Meißner, Constraints on the chiral unitary  $\bar{K}N$  amplitude from  $\pi\Sigma K^+$  photoproduction data, *Eur. Phys. J. A* **51**, 30 (2015).
- [11] L. Roca and E. Oset, Isospin 0 and 1 resonances from  $\pi\Sigma$  photoproduction data, *Phys. Rev. C* **88**, 055206 (2013).
- [12] G. Scheluchin *et al.* (BGOOD Collaboration), Photoproduction of  $K^+\Lambda(1405) \rightarrow K^+\pi^0\Sigma^0$  extending to forward angles and low momentum transfer, *Phys. Lett. B* **833**, 137375 (2022).
- [13] N. Wickramaarachchi, R. A. Schumacher, and G. Kalicy (GlueX), Decay of the  $\Lambda(1405)$  hyperon to  $\Sigma^0\pi^0$  measured at GlueX, *EPJ Web Conf.* **271**, 07005 (2022).
- [14] S. Acharya *et al.* (ALICE Collaboration), Constraining the  $\bar{K}N$  coupled channel dynamics using femtoscopic correlations at the LHC, *Eur. Phys. J. C* **83**, 340 (2023).
- [15] S. Aikawa *et al.* (J-PARC E31 Collaboration), Pole position of  $\Lambda(1405)$  measured in  $d(K^-, n)\pi\Sigma$  reactions, *Phys. Lett. B* **837**, 137637 (2023).
- [16] A. V. Anisovich, A. V. Sarantsev, V. A. Nikonov, V. Burkert, R. A. Schumacher, U. Thoma, and E. Klempt, Hyperon III:  $K^-p - \pi\Sigma$  coupled-channel dynamics in the  $\Lambda(1405)$  mass region, *Eur. Phys. J. A* **56**, 139 (2020).
- [17] N. Isgur and G. Karl, P wave baryons in the quark model, *Phys. Rev. D* **18**, 4187 (1978).
- [18] N. Kaiser, P. B. Siegel, and W. Weise, Chiral dynamics and the low-energy kaon—nucleon interaction, *Nucl. Phys.* **A594**, 325 (1995).
- [19] E. Oset and A. Ramos, Nonperturbative chiral approach to  $s$  wave  $\bar{K}N$  interactions, *Nucl. Phys.* **A635**, 99 (1998).
- [20] A. Martinez Torres, M. Bayar, D. Jido, and E. Oset, Strategy to find the two  $\Lambda(1405)$  states from lattice QCD simulations, *Phys. Rev. C* **86**, 055201 (2012).
- [21] S. Weinberg, Pion scattering lengths, *Phys. Rev. Lett.* **17**, 616 (1966).
- [22] Y. Tomozawa, Axial vector coupling renormalization and the meson baryon scattering lengths, *Nuovo Cimento A* **46**, 707 (1966).
- [23] J. A. Oller and U. G. Meissner, Chiral dynamics in the presence of bound states: Kaon nucleon interactions revisited, *Phys. Lett. B* **500**, 263 (2001).
- [24] M. Mai, Status of the  $\Lambda(1405)$ , *Few Body Syst.* **59**, 61 (2018).
- [25] M. Mai, Review of the  $\Lambda(1405)$  A curious case of a strangeness resonance, *Eur. Phys. J. Special Topics* **230**, 1593 (2021).
- [26] U.-G. Meißner, Two-pole structures in QCD: Facts, not fantasy!, *Symmetry* **12**, 981 (2020).
- [27] T. Ezo and A. Hosaka,  $\Lambda(1405)$  as a  $\bar{K}N$  Feshbach resonance in the Skyrme model, *Phys. Rev. D* **102**, 014046 (2020).
- [28] K. S. Myint, Y. Akaishi, M. Hassanvand, and T. Yamazaki, Single-pole nature of the detectable  $\Lambda(1405)$ , *Prog. Theor. Exp. Phys.* **2018**, 073D01 (2018).
- [29] K. Miyahara, T. Hyodo, and W. Weise, Construction of a local  $\bar{K}N - \pi\Sigma - \pi\Lambda$  potential and composition of the  $\Lambda(1405)$ , *Phys. Rev. C* **98**, 025201 (2018).
- [30] K. Miyahara and T. Hyodo, Theoretical study of  $\Lambda(1405)$  resonance in  $\Xi_b^0 \rightarrow D^0(\pi\Sigma)$  decay, *Phys. Rev. C* **98**, 025202 (2018).
- [31] K. Azizi, Y. Sarac, and H. Sundu, Investigation of  $\Lambda(1405)$  as a molecular pentaquark state, [arXiv:2306.07393](https://arxiv.org/abs/2306.07393).
- [32] J.-M. Xie, J.-X. Lu, L.-S. Geng, and B.-S. Zou, Two-pole structures demystified: Chiral dynamics at work, [arXiv:2307.11631](https://arxiv.org/abs/2307.11631).
- [33] J.-X. Lu, L.-S. Geng, M. Doering, and M. Mai, Cross-channel constraints on resonant antikaon-nucleon scattering, *Phys. Rev. Lett.* **130**, 071902 (2023).
- [34] T. Hyodo and W. Weise, Theory of Kaon-Nuclear Systems, in *Handbook of Nuclear Physics*, edited by I. Tanihata, H. Toki, and T. Kajino (Springer, Singapore, 2022), pp. 1–34, [10.1007/978-981-15-8818-1\\_38-1](https://doi.org/10.1007/978-981-15-8818-1_38-1).
- [35] D. Jido, J. A. Oller, E. Oset, A. Ramos, and U. G. Meissner, Chiral dynamics of the two  $\Lambda(1405)$  states, *Nucl. Phys.* **A725**, 181 (2003).
- [36] R. Molina and M. Döring, Pole structure of the  $\Lambda(1405)$  in a recent QCD simulation, *Phys. Rev. D* **94**, 056010 (2016); **94**, 079901(A) (2016).
- [37] M. Lüscher, Two particle states on a torus and their relation to the scattering matrix, *Nucl. Phys.* **B354**, 531 (1991).
- [38] K. Rummukainen and S. A. Gottlieb, Resonance scattering phase shifts on a nonrest frame lattice, *Nucl. Phys.* **B450**, 397 (1995).
- [39] C. H. Kim, C. T. Sachrajda, and S. R. Sharpe, Finite-volume effects for two-hadron states in moving frames, *Nucl. Phys.* **B727**, 218 (2005).
- [40] S. He, X. Feng, and C. Liu, Two particle states and the S-matrix elements in multi-channel scattering, *J. High Energy Phys.* **07** (2005) 011.
- [41] V. Bernard, M. Lage, U. G. Meissner, and A. Rusetsky, Scalar mesons in a finite volume, *J. High Energy Phys.* **01** (2011) 019.
- [42] M. Göckeler, R. Horsley, M. Lage, U. G. Meißner, P. E. L. Rakow, A. Rusetsky, G. Schierholz, and J. M. Zanotti, Scattering phases for meson and baryon resonances on general moving-frame lattices, *Phys. Rev. D* **86**, 094513 (2012).
- [43] R. A. Briceno and Z. Davoudi, Moving multichannel systems in a finite volume with application to proton-proton fusion, *Phys. Rev. D* **88**, 094507 (2013).
- [44] R. A. Briceno, Two-particle multichannel systems in a finite volume with arbitrary spin, *Phys. Rev. D* **89**, 074507 (2014).
- [45] P. Gubler, T. T. Takahashi, and M. Oka, Flavor structure of  $\Lambda$  baryons from lattice QCD: From strange to charm quarks, *Phys. Rev. D* **94**, 114518 (2016).
- [46] B. J. Menadue, W. Kamleh, D. B. Leinweber, and M. S. Mahbub, Isolating the  $\Lambda(1405)$  in lattice QCD, *Phys. Rev. Lett.* **108**, 112001 (2012).
- [47] G. P. Engel, C. B. Lang, and A. Schäfer (BGR (Bern-Graz-Regensburg) Collaboration), Low-lying  $\Lambda$  baryons from the lattice, *Phys. Rev. D* **87**, 034502 (2013).

- [48] G. P. Engel, C. B. Lang, D. Mohler, and A. Schäfer (BGR Collaboration), QCD with two light dynamical chirally improved quarks: Baryons, *Phys. Rev. D* **87**, 074504 (2013).
- [49] Y. Nemoto, N. Nakajima, H. Matsufuru, and H. Suganuma, Negative parity baryons in quenched anisotropic lattice QCD, *Phys. Rev. D* **68**, 094505 (2003).
- [50] T. Burch, C. Gattringer, L. Y. Glozman, C. Hagen, D. Hierl, C. B. Lang, and A. Schafer, Excited hadrons on the lattice: Baryons, *Phys. Rev. D* **74**, 014504 (2006).
- [51] T. T. Takahashi and M. Oka, Low-lying lambda baryons with spin 1/2 in two-flavor lattice QCD, *Phys. Rev. D* **81**, 034505 (2010).
- [52] S. Meinel and G. Rendon, Charm-baryon semileptonic decays and the strange  $\Lambda^*$  resonances: New insights from lattice QCD, *Phys. Rev. D* **105**, L051505 (2022).
- [53] J. M. M. Hall, W. Kamleh, D. B. Leinweber, B. J. Menadue, B. J. Owen, A. W. Thomas, and R. D. Young, Lattice QCD evidence that the  $\Lambda(1405)$  resonance is an antikaon-nucleon molecule, *Phys. Rev. Lett.* **114**, 132002 (2015).
- [54] M. Fukugita, Y. Kuramashi, M. Okawa, H. Mino, and A. Ukawa, Hadron scattering lengths in lattice QCD, *Phys. Rev. D* **52**, 3003 (1995).
- [55] W. Detmold and A. N. Nicholson, Low energy scattering phase shifts for meson-baryon systems, *Phys. Rev. D* **93**, 114511 (2016).
- [56] A. Torok, S. R. Beane, W. Detmold, T. C. Luu, K. Orginos, A. Parreno, M. J. Savage, and A. Walker-Loud, Meson-baryon scattering lengths from mixed-action lattice QCD, *Phys. Rev. D* **81**, 074506 (2010).
- [57] G.-W. Meng, C. Miao, X.-N. Du, and C. Liu, Lattice study on kaon nucleon scattering length in the  $I = 1$  channel, *Int. J. Mod. Phys. A* **19**, 4401 (2004).
- [58] J. Bulava, B. Cid-Mora, A. D. Hanlon, B. Hörz, D. Mohler, C. Morningstar, J. Moscoso, A. Nicholson, F. Romero-López, S. Skinner, and A. Walker-Loud (Baryon Scattering (BaSc) Collaboration), companion paper, Lattice QCD study of  $\pi\Sigma - \bar{K}N$  scattering and the  $\Lambda(1405)$  resonance, *Phys. Rev. D* **109**, 014511 (2024).
- [59] M. Bruno *et al.*, Simulation of QCD with  $N_f = 2 + 1$  flavors of non-perturbatively improved Wilson fermions, *J. High Energy Phys.* **02** (2015) 043.
- [60] M. Bruno, T. Korzec, and S. Schaefer, Setting the scale for the CLS 2 + 1 flavor ensembles, *Phys. Rev. D* **95**, 074504 (2017).
- [61] B. Strassberger *et al.*, Scale setting for CLS 2 + 1 simulations, *Proc. Sci., LATTICE2021* (2022) 135 [arXiv:2112.06696].
- [62] C. Morningstar, J. Bulava, J. Foley, K. J. Juge, D. Lenkner, M. Peardon, and C. H. Wong, Improved stochastic estimation of quark propagation with Laplacian Heaviside smearing in lattice QCD, *Phys. Rev. D* **83**, 114505 (2011).
- [63] J. Bulava, A. D. Hanlon, B. Hörz, C. Morningstar, A. Nicholson, F. Romero-López, S. Skinner, P. Vranas, and A. Walker-Loud, Elastic nucleon-pion scattering at  $m_\pi = 200$  MeV from lattice QCD, *Nucl. Phys.* **B987**, 116105 (2023).
- [64] B. Hörz and A. Hanlon, Two- and three-pion finite-volume spectra at maximal isospin from lattice QCD, *Phys. Rev. Lett.* **123**, 142002 (2019).
- [65] C. Morningstar, J. Bulava, B. Singha, R. Brett, J. Fallica, A. Hanlon, and B. Hörz, Estimating the two-particle  $K$ -matrix for multiple partial waves and decay channels from finite-volume energies, *Nucl. Phys.* **B924**, 477 (2017).
- [66] P. Guo, J. J. Dudek, R. G. Edwards, and A. P. Szczepaniak, Coupled-channel scattering on a torus, *Phys. Rev. D* **88**, 014501 (2013).
- [67] J. M. Blatt and L. C. Biedenharn, Neutron-proton scattering with spin-orbit coupling. 1. General expressions, *Phys. Rev.* **86**, 399 (1952).
- [68] G. Källén, *Elementary Particle Physics* (Addison-Wesley, Reading, MA, 1964).
- [69] C. R. Harris, K. J. Millman, S. J. Van Der Walt, R. Gommers, P. Virtanen, D. Cournapeau, E. Wieser, J. Taylor, S. Berg, N. J. Smith *et al.*, Array programming with numpy, *Nature (London)* **585**, 357 (2020).
- [70] J. D. Hunter, Matplotlib: A 2d graphics environment, *Comput. Sci. Eng.* **9**, 90 (2007).
- [71] R. G. Edwards and B. Joo (SciDAC Collaboration), The Chroma software system for lattice QCD, *Nucl. Phys. B, Proc. Suppl.* **140**, 832 (2005).
- [72] S. Kuberski, Low-mode deflation for twisted-mass and RHMC reweighting in lattice QCD, arXiv:2306.02385.
- [73] D. Stanzione, J. West, R. Evans, T. Minyard, O. Ghattas, and D. Panda, Frontera: The evolution of leadership computing at the National Science Foundation, in *Proceedings of Practice and Experience in Advanced Research Computing (PEARC '20)* (ACM, New York, 2020).